Properties of

CCD #4

installed in dewar no. 2
Operated as HiRAC science camera.

Anton Norup Sørensen & Michael I. Andersen
Copenhagen University Observatory

December 1996

1 Introduction

The BroCamII (dewar no. 2) was commissioned at the Nordic Optical Telescope (NOT) in January 1996, but had to be withdrawn during the summer due to a CCD malfunction from thermal stress.

This document describes the performance of the camera at the re-commissioning in December 1996 with a new CCD, wafer W14-2, at NOT known as CCD #4.

The CCD is a Ford-Loral three side buttable with 2048^2 imaging pixels. Packaging for back-side illumination, "ultra-thinning" and coating was performed by the Steward Observatory CCD Laboratory. The coating consists of HfO_2 for anti-reflection and PPtF for back-side charging, essential for good blue sensitivity.

2 Operating options

The CCD has two functional output amplifiers, 'A' and 'B'. These can be selected individually or used simultaneously. Default is 'A' only. Before using both amplifiers simultaneously, one should consider the consequences of cross-talk and a more complicated reduction due to different gain and bias behavior.

The parallel phases can be operated in "normal" (type "mpp-" to set) or "mpp" mode (type "mpp+" to set). Default is mpp, where dark current is minimized.

Operating temperature is normally -100° C, and testing has only been performed at this temperature.

Two ADU conversion factors can be selected, "high" or "low". "high" gain is default and offers the best signal to noise ratio at the expense of a slightly reduced dynamic range.

The area to be read out may be specified by any rectangular section, and on-chip pixel binning may be specified independently in the x and y directions.

While three types of overscan can be selected, only one of them is reliable. Size is programmable, but it is required that the read-out window extends to one edge of the CCD in the X-direction.

3 Cosmetics

Flat fields at different wavelengths are shown in figures 6, 7 and 8. Large scale uniformity is very good at visual and UV wavelengths, with peak to peak variations of 3%. Around $1\mu m$ the non-uniformities increase to 10%. At the extreme corners and edges, sensitivity goes down as the chip is not thinned here. An X-like structure is seen from corner to corner - this is most probably light reflected off the concave border of the thinned area at the corners.

Specks a few pixels wide having reduced sensitivity are scattered over the entire imaging area. Setting a threshold 3% lower than the median sensitivity, 1% of the area is affected by the specks. The central sensitivity typically goes down by 20%, but a few areas goes much lower. All of the specks can be corrected by flat-fielding.

Charge traps and bad columns can be found by comparing a flat field exposure at very low illumination level to a well exposed one, as illustrated in figure 1. In the table below, the coordinates of defects found are listed. Note that the number of pixels affected by a trap depends on the illumination. The actual trap location is the smallest Y-coordinate of the area.

Low level traps	**Comment**
$[435:435, 1739:1744]$	
$[566, 566, 492:496]$	
$[936:937, 1093:1152]$	Previously a light emitting pixel here in mpp- mode
$[1056:1056, 1015:1019]$	
$[1581:1581, 17:19]$	
$[1286:1286, 1052:1067]$	
$[2001:2001, 1321:1338]$	
$[1408:1408, 1643:1707]$	
High level traps or bad columns	
$[1834:1836, 1388:2050]$	
$[1041:1042, 1254:2050]$	
$[936:936, 1092:2050]$	Flat field OK above trap?
$[965:966:355:357]$	
$[965:965:355:2050]$	Flat field OK?
Other	
$[1492:1495, 743:747]$	Worst of low sensitivity specks
$[1388:1388, 1190:2050]$	Hot pixel and warm column in darks

4 Read-out noise

Noise measured in bias frames with 1*1 binning, mpp+ mode, amounts to:

	Amplifier A	Amplifier B
High gain:	6.25 e^-	6.35 e^-
Low gain:	7.55 e^-	8.20 e^-

While the values above were obtained for 1 by 1 pixel binning, read out at higher binning is disturbed by a pattern visible in low exposure level frames. By careful reduction it may be possible to eliminate this pattern, but if the pattern is left uncorrected, the resulting high gain read-out noise becomes:

Binning	Amplifier A	Amplifier B
1*1:	6.3 e^-	6.4 e^-
2*2:	6.3 e^-	6.4 e^-
3*3:	6.3 e^-	15.0 e^-
4*4:	8.9 e^-	15.0 e^-

The mpp- mode seems to result in higher read-out noise, e.g. Amplifier A, high gain, mpp-, 1*1 binning has 7.5 e^- RON.

When using amplifier B, the noise in the rightmost part of the read-out window is increased by about 20% by lines of fluctuating length, up to about 100 pixels, with a slightly different level.

5 Cross-talk

In dual read-out mode, cross-talk occurs between the two amplifiers. An image of a star in one side of the image will then have a fainter electronic ghost image mirrored around the border of the two image sections.

Making photometry on the image and ghost image of the HiRAC artificial star, the following cross-talk strengths was found:

Signal in B channel from A channel: $1.5 \cdot 10^{-4}$

Signal in A channel from B channel: $1.9 \cdot 10^{-4}$

6 Gain, linearity and full-well

From analysis of photon noise statistics, the following conversion factors were found:

	Amplifier A	Amplifier B
High gain:	1.14 e^-/ADU	1.08 e^-/ADU
Low gain:	3.1 e^-/ADU	3.0 e^-/ADU

Gain measured from Poisson noise statistics shows a strong dependency on the exposure level on some CUO cameras. For the W11-4, the relation found is plotted in figure 2, indicating a deviation from linearity of about 3%.

A more precise measurement of linearity is reached by measuring the ADU level versus exposure time, using a stable light source. Measurements made in this way are plotted in figure 3. By dividing the counts with the exposure time, corrected for a shutter delay of 0.12 second, a significant linearity deviation is found. The amplitude is 0.7% over the entire high-gain dynamic range. Almost the same shape and amplitude of the deviation is found for both amplifiers, in both high and low gain mode. For high-precision photometry, this must be corrected for. Apparently, a simple correction as suggested below will suffice.

$$ADU_{corrected} = ADU_{raw} \cdot (1 - c \cdot \frac{ADU_{raw}}{65535})$$

Where c is:

	Amplifier A	Amplifier B
High gain:	0.007	0.008
Low gain:	0.009	0.011

The Poisson noise analysis clearly goes wrong: it finds a deviation of the wrong amplitude and even of the wrong sign. A noise modulation/source must be causing this, but the origin is currently unknown.

Full well: Saturation occurs at approx. 105.000 e^- for both channels. At 90.000 e^-, corresponding to 30.000 ADU in low gain mode and above the dynamic range of high gain mode, no saturation effects are seen. Surprisingly, the full well is independent of the mpp mode.

7 Charge transfer efficiency

The fraction of electrons that are successfully moved from one pixel to another during read-out is described by the charge transfer efficiency (CTE).

The CTE has been measured using a ^{55}Fe X-ray source, whose emissions generate a specific number of photo-electrons on the CCD for each detection. The read-out counts as a function of position on the CCD can then be converted to a CTE value.

The values found are:

Serial CTE:	1.000000
Parallel CTE:	0.999997

Transporting the charge from the most remote corner of the CCD to the output amplifier will then lead to a 0.6% loss of charge

Note that CTE strictly speaking is a function of exposure level, so the value given here may not be applicable to all cases. Near zero level and full well, CTE can be expected to be poorer.

8 Modulation Transfer Function

The potential well of the pixel-defining electrodes does not extend all the way to the surface of the CCD. Photo-electrons generated near the surface may then diffuse to neighbor pixels, causing a degradation of the image sharpness. The CCD #4 has been "ultra thinned" to reduce this problem, but measurements of the Modulation Transfer Function made by [Andersen, M. I. 96] shows the problem still is significant.

The measurement displayed in figure 4 is made at 632 nm. The degradation is expected to be worse at shorter wavelengths and vice versa due to the color-dependent transparency of the CCD. From this, an effective pixel size in excess of 2 physical pixels is inferred.

9 Pt-pinning and quantum-efficiency

In order to reach high quantum efficiency at short wavelengths, the CCD is coated to create a "passivated" Platinum flash gate. This adsorbs O_2^- ions when in an Oxygen atmosphere, which causes the back side to become negatively charged. The photo-electrons generated near the surface of the CCD are repelled and forced towards the electrodes before recombination occurs.

When the dewar becomes warm, outgassing of hydrocarbons occurs. These combine with the O_2^- ions and cancel the negative surface charge, leaving the CCD insensitive to short wavelength photons.

Procedure for Oxygen soaking:

After exposure to outgassing components or humid air, QE is restored in the following way:

Let the camera heat up to room temperature by setting the CCD reference temperature to +20° C before the remaining liquid Nitrogen is used. As strong outgassing occurs, the camera should be pumped during the heating and must be pumped for at least an hour when warm. The camera is then filled with dry air to about ambient pressure. In order to ensure no other air enters, a T-tube must be connected to the dewar valve with the the other ends going to the dry air bottle and a vacuum pump. If the pump is not equipped with a valve, one must be inserted. The tube between the the cryostat and bottle is then evacuated, the valve to the cryostat opened, removing outgassing components from the warm camera. The valve to the pump is closed, and dry air can now slowly be let in while monitoring the camera pressure closely. Fill the camera to slightly less than ambient pressure, then close the cryostat valve. Leave the camera with dry air at room temperature for at least an hour, then evacuate and cool with LN_2. The QE is now restored to specifications.

Quantum efficiency vs. wavelength: With backside charging and a HfO_2 coating, the QE reaches it's maximum value of approx. 90% from 400nm to 550nm, as can be seen in the QE vs. wavelength plot in figure 5. Within the uncertainties of the absolute calibration, the CUO and Steward Observatory Lab measurements are in good agreement from 550nm and shortwards, considering an uncertainty of about 10% of the 366nm CUO measurements. At longer wavelengths, the measurements differ because of the temperature of the CCD: room temperature for the SOL measurements and -100° C for the CUO measurements. At high temperatures, the extra thermal energy of the lattice makes the electrons easily excitable by low energy photons, but the cost is a dramatically increased dark current. For observations in the $1.0\mu m$ to $1.1\mu m$ range, one might try using a CCD temperature of -80° C.

Stability of the sensitivity:

Measurements performed at November 20 and 28 in figure 5 are both made 20 hours after Oxygen soaking and cooling. The identical curves show that a repeatable level is reached. 8 days after cooling the global QE remains at the same level, as shown by the December 6 graph. While the stability is excellent while the CCD is cold and in vacuum, the backside charge is completely destroyed by the outgassing that occurs at exhaustion of the liquid Nitrogen supply. This is illustrated by the October 23 graph, where the CCD was warmed up for one day and then cooled again without Oxygen soaking or pumping.

In order to check whether the QE is still at the original level, a blue beta-fluorescent source can be placed in the filter wheel for a reference exposure. On December 15 '96, a few hours after soaking and cooling, a level of 57900 ADU was found in the central part of an image after bias subtraction. The image was made with the settings: high gain, amplifier A, binning 1 by 1. The estimated temperature was $+10°$ C. The source intensity is claimed to have a $-0.3\%/K$ temperature dependency, and also looses 6% every year due to the radioactive decay.

Flat field images at 1060nm, 550nm and 366nm illumination were obtained regularly during the cold period after soaking and cooling. Also local structure of the flat fields remains constant, as can be seen from the flat fields displayed in figures 6, 7 and 8. The pairs of flat fields are obtained 20 hours after and 8 days after cooling, and the ratio between the images sets an upper limit to the change in structure of 0.1% for the 1060nm and 550nm images and a limit of 1% at 366nm due to the lower signal to noise ratio. The only problem appears to be to keep dust away from the dewar window and filters!

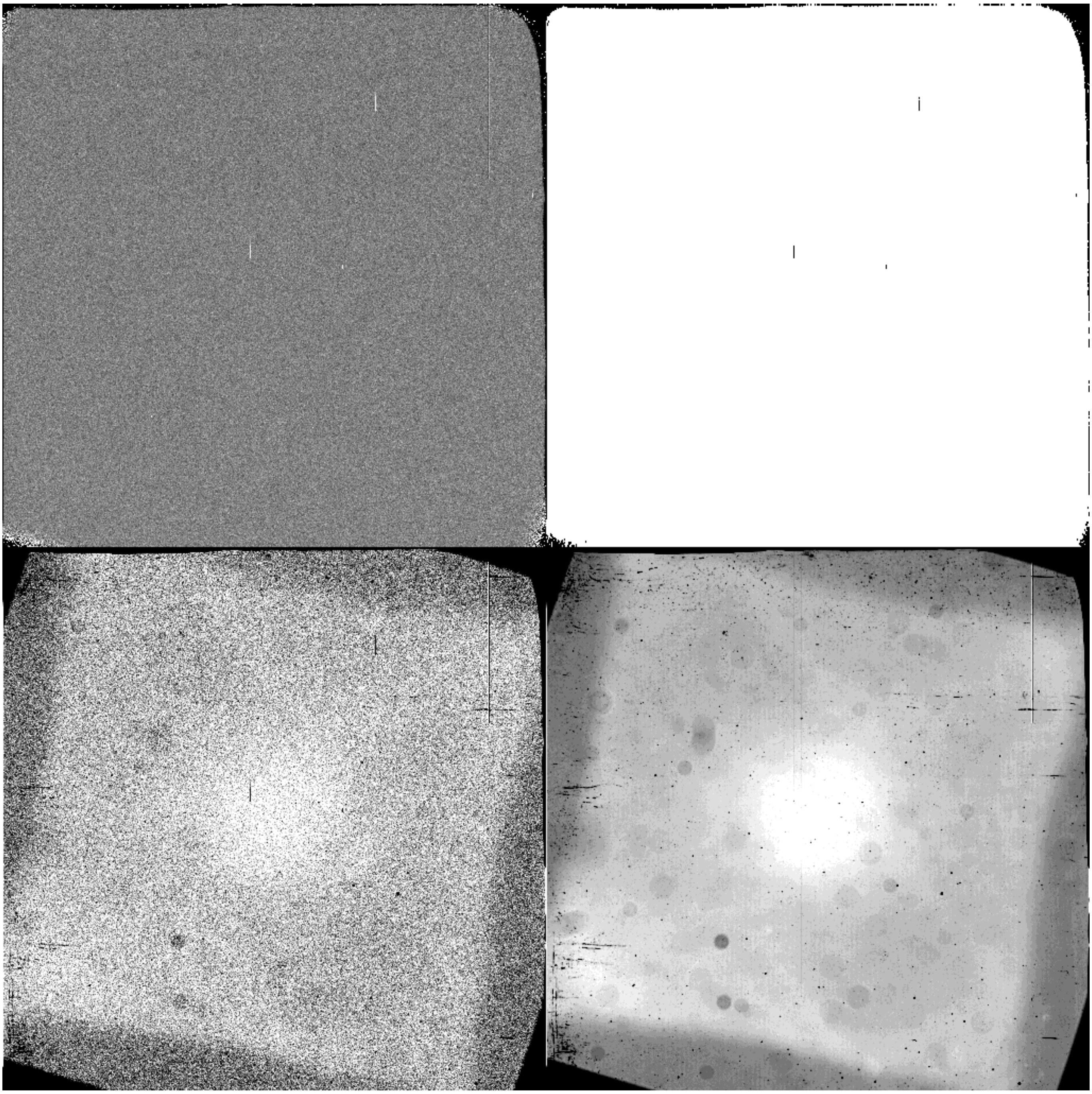

Figure 1: Low illumination level flat field properties, as a mean of identifying charge traps. *Lower left:* Flat field at an illumination level of $74e^{-}$/pixel. Grey scale cuts are $\pm$ 5% of median level. *Lower right:* Flat field at an illumination level of $40.000e^{-}$/pixel. The tilted square and central blob structure are caused by stray light in the setup. *Upper left:* Ratio of the two flat fields. The bright vertical lines show areas affected by low level traps. Grey scale cuts are $\pm$ 15% of median level. *Upper right:* Different cuts applied to the ratio image, emphasizing traps

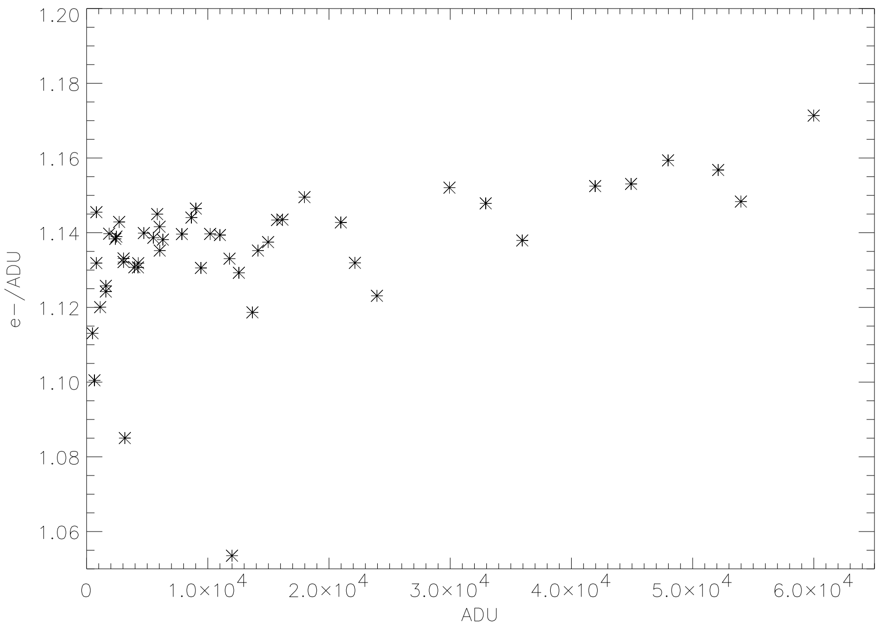

Figure 2: Gain versus exposure level measured from noise statistics for amplifier A in high-gain. The gain apparently changes by 3% over the dynamic range, but change is shown to be smaller by the more precise measurement plotted in figure 3.

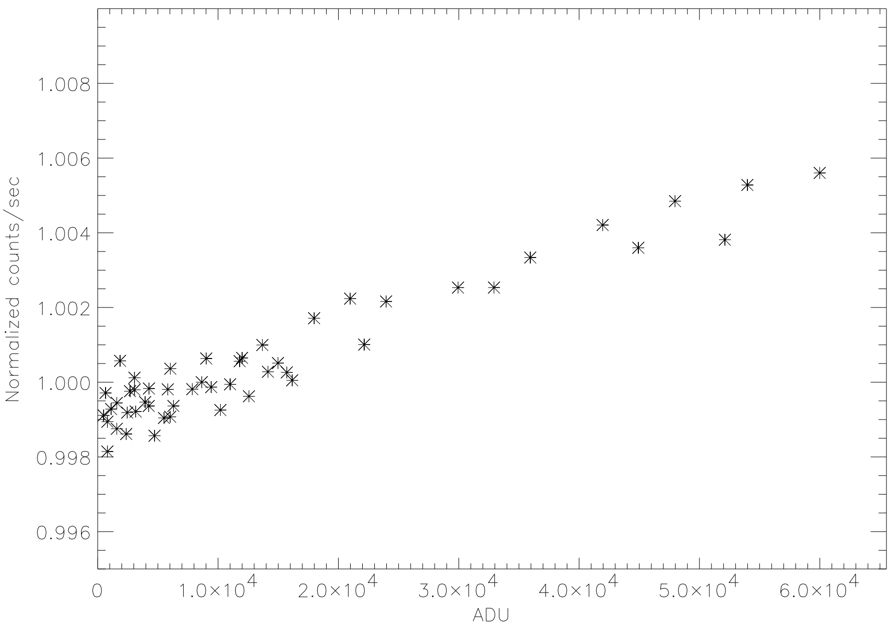

Figure 3: A plot of ADU per second versus total exposure time, corrected for shutter delay. By using a stable light source, the scatter becomes small enough to reveal a linearity deviation of 0.7% over the dynamic range for amplifier A in high gain mode.

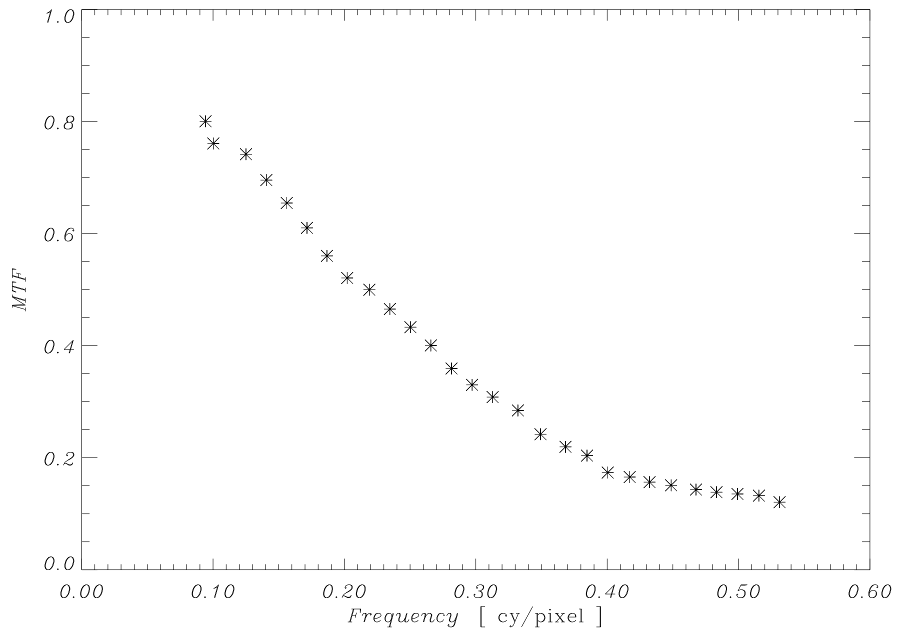

Figure 4: MTF of the CCD #4 measured at a wavelength of 632nm. Compared to the ideal sinc-shaped MTF of a pixel, the measured MTF represents a severe loss of resolution.

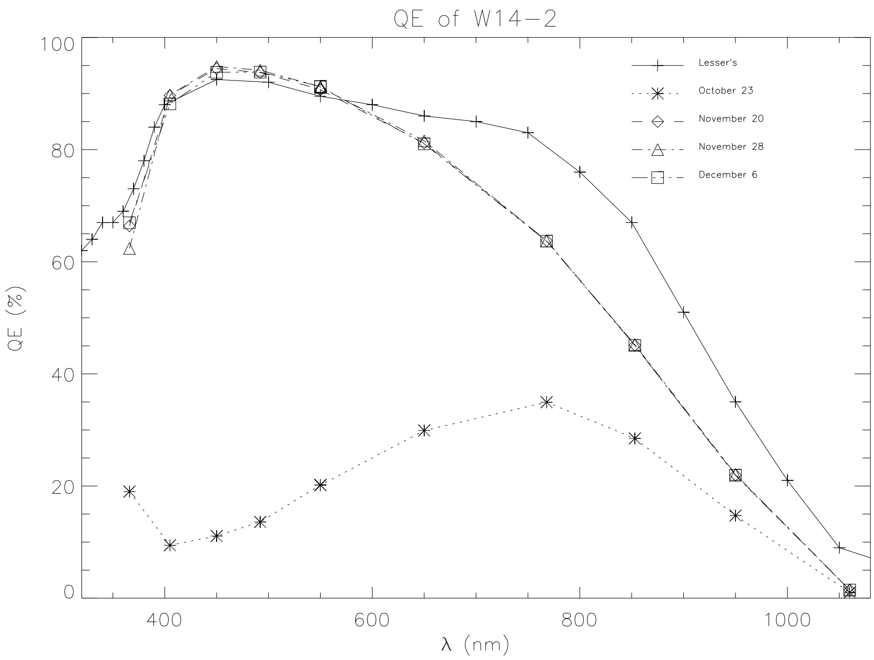

Figure 5: Quantum efficiency of the CCD #4. Solid line with crosses is the measurement performed by the Steward Lab. at room temperature. The three almost coincident curves obtained at -100° C at the CUO lab. shows the excellent stability when the camera is kept cold. The lower curve shows the poor QE after "Hydrogen poisoning". The measurements at 366nm have an uncertainty of about 10%.

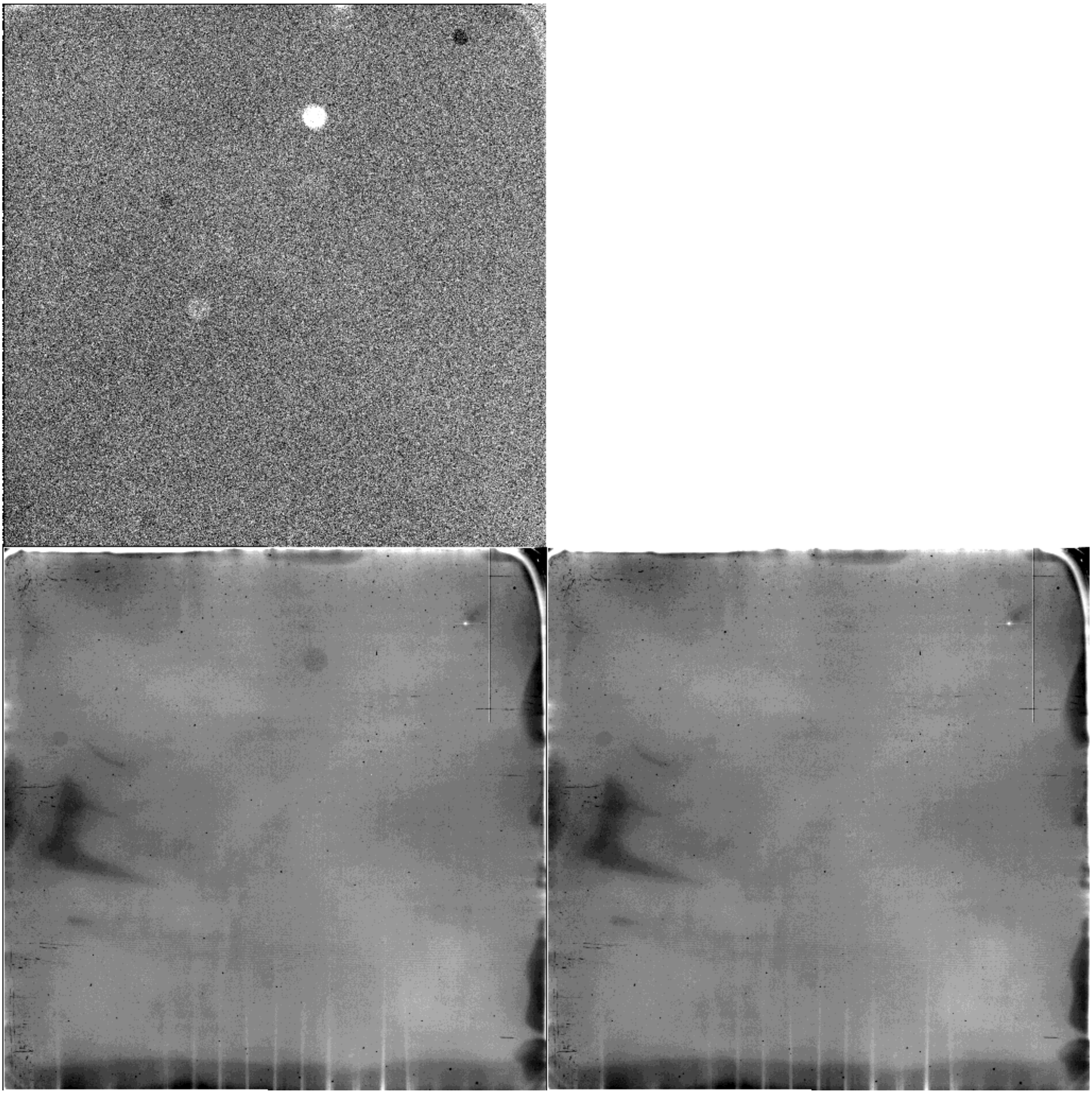

Figure 6: Flat field properties at 1060nm. *Lower left:* 20 hours after cooling. The greyscale cuts are set to $\pm 10\%$ of the median level. The large scale structure with a peak to peak amplitude of about 10 % directly relates to the thickness of the CCD, almost completely transparent at this wavelength. The vertical lines at the bottom is light reflected off electrodes below the CCD. The low sensitivity specks are relatively faint. *Lower right:* 8 days after cooling. *Upper left:* Ratio between the two flat fields, displayed with cuts of $\pm 1\%$. Except for a few displaced dust specks, the flat field is unchanged to within 0.1%

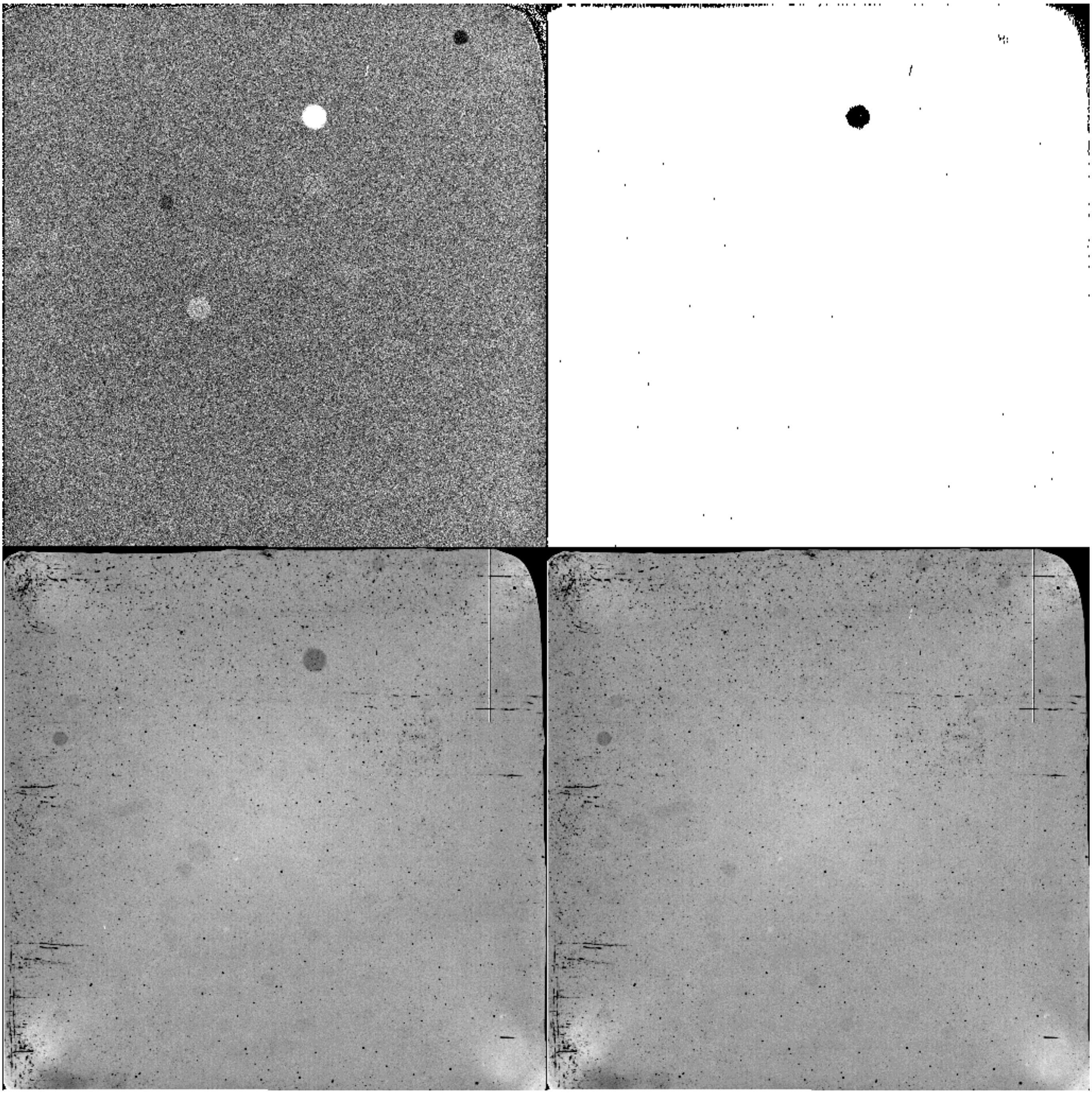

Figure 7: Flat field properties at 550nm. *Lower left:* 20 hours after cooling. The greyscale cuts are set to ±5% of the median level. The "X" pattern extending from corner to corner is probably stray light reflected off the rounded corners, and the central bulge may also be due to stray light. Peak to peak large scale structure is about 2%. *Lower right:* 8 days after cooling. *Upper left:* Ratio between the two flat fields, displayed with cuts of ±1%. Except for a few displaced dust specks, the flat field is unchanged to within 0.1%

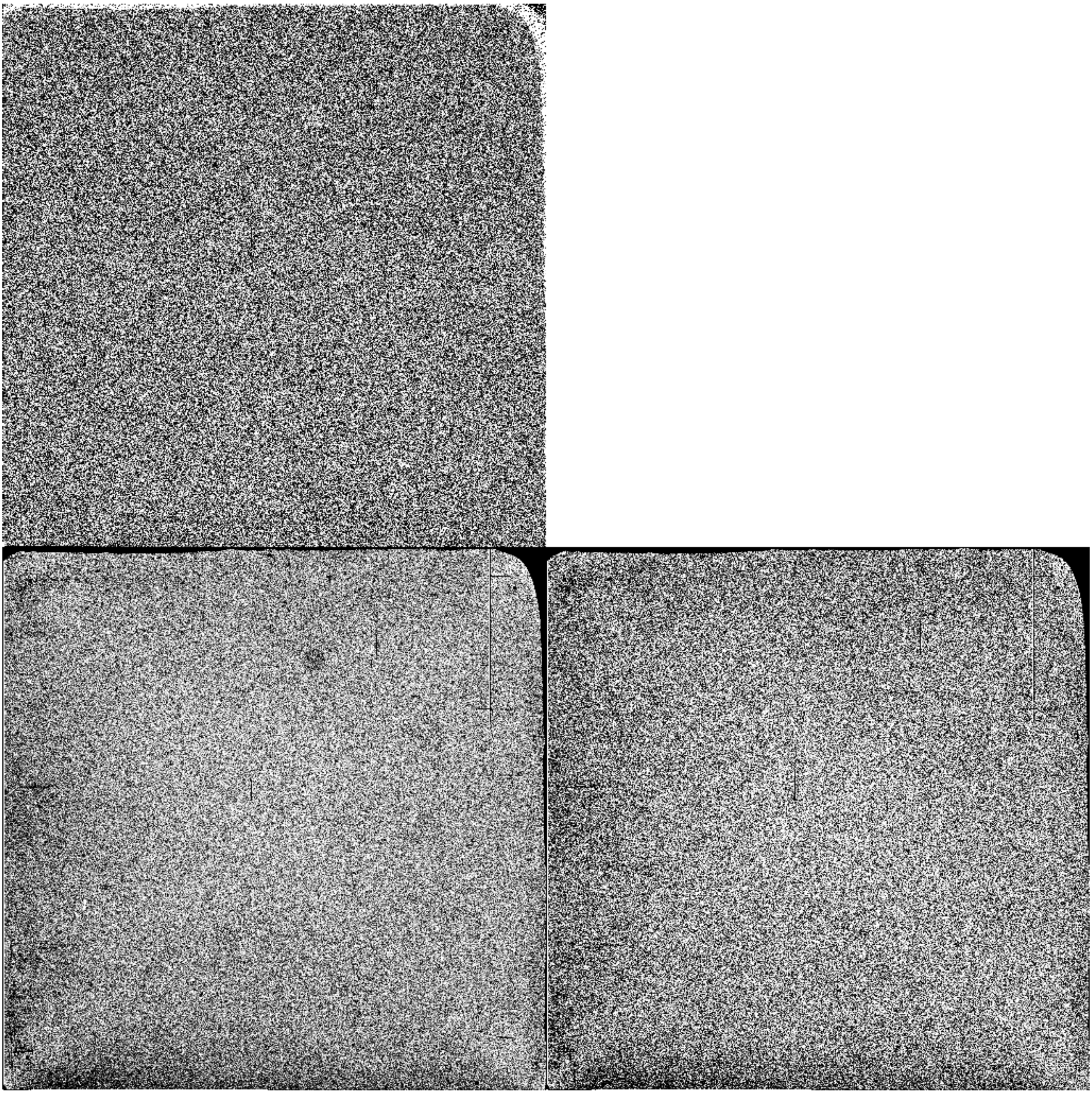

Figure 8: Flat field properties at 366nm. *Lower left:* 20 hours after cooling. The greyscale cuts are set to $\pm 5\%$ of the median level. Peak to peak large scale structure is about 3%. *Lower right:* 8 days after cooling. *Upper left:* Ratio between the two flat fields, displayed with cuts of $\pm 5\%$. No changes down to an amplitude of 1% are seen.

10 Bias and overscan

The CCD controller has been modified with the goal of achieving bias frames with a flatter shape and higher reproduceabilty. A comparison between two bias frames is shown in figure 9. One bias is made after the camera has been idle for an hour, and the other is made after a few minutes of constant read-out activity. The high similarity of the two frames indicate a very stable bias.

The CCD has "register" overscan regions of two columns at each end of the serial register. These areas somewhat too small for a high signal to noise measurement and are suspected to be affected by the illumination of the imaging area, so they are not recommended as bias level reference.

The recommended type of "extended clocking" overscan can only be used for read-out windows extending to the edge of the CCD opposite of the amplifier being used. Overscan in the X-direction is set by the "xover" command, and in the Y-direction by "yover". The Y-overscan is of little practical use, though. To get the overscan region in the image, the window size must be specified to go beyond the border of the CCD by the width of the overscan. E.g. An image of the section [1500:2052,something] with a X-overscan width of 50 using the A-amplifier would be defined like this:

ampl A
xover 50
xbeg 1500
xsiz 602 (i.e. $2052 - 1500 + 50$)

To make a window with overscan using the B amplifier, the area must include the left border. E.g. [1:500,something] with an X-overscan of 50 would be set up like:

ampl B
xover 50
xbeg 0
xsiz 550 (i.e. $500 + 50$)

The default x-overscan size is 50 and zero in the y-direction. Post-processing by BIAS will always make the x-overscan appear at the right border of the image, whatever amplifier is specified.

The overscan level has been confirmed not to drift relatively to the bias level as a function of exposure time. There is a small drift with illumination, practically neglectable with an amplitude of 2 ADU for near-saturation illumination.

Another type of "synthetic" overscan can be defined by the "over" command. This type can be used for any window geometry, but has proved to be very unreliable. It should not be used under any circumstances, so do not change the default size of zero.

The bias level is approximately 400 ADU, but changes a little depending on the amplifier, gain and mpp mode selection.

11 Saturation residuals

If you illuminate the CCD strongly without making an exposure, like may be happening when filters are mounted, the normal pre-clear before an exposure is not sufficient. In this situation, the first image taken afterwards will have a gradient in the vertical direction and an increased background level. Gross saturation during normal exposures, followed by read-out, will not affect the next image.

12 Dark current

A 20 minute dark exposure made in mpp+ mode at -100° C is shown in figure 10. The image has not been bias subtracted. Along the edges, dark current is increased where the CCD is not thinned, as here is more Silicon in which a spontaneous free electron can appear. Almost no cosmic hits appear as single pixel events, due to the MTF problem. A group of hot pixels are around (1388,1190), also increasing the level of the column at this location.

In mpp+ mode, the dark current is measured to $1e^-$/hour, while in mpp- mode the dark current increases to $6e^-$/hour.

13 Analog to Digital Converter

Imperfections in the digitization of the CCD output voltage are causing some ADU values to appear more frequently than others, as can be seen in figure 11. The additional noise may be detectable on exposures with very little signal, where the noise normally would be read-out-noise limited. With a few hundred counts or more, the photon noise will dominate the noise from the ADC.

14 Pixel size

By illuminating the CCD with collimated light through a grid of pinholes with known separation, the following dimensions were found for a CCD from the same batch as CCD #4:

Pixel size in serial direction:	$15.03 \pm 0.02\mu m$
Pixel size in parallel direction:	$14.99 \pm 0.01\mu m$

This is consistent with the design specifications of $15\mu m$ square pixels.

15 Cryostat

With the camera mounted on the telescope, the filling inlet of the dewar will be pointing downwards. An inner tube must be mounted in the cryostat - otherwise no liquid Nitrogen can be stored. Pointing the telescope at Zenith will allow complete filling with a holding time of about 30 hours. Observing close to the horizon will cause up to half of the Nitrogen to spill out, implying a proportional reduction in holding time. The LN_2 temperature displayed in the BIAS CCD status window is a good indicator of the amount of Nitrogen in the cryostat. A completely full tank will make a temperature of slightly below -198° C being displayed. As the temperature sensor is placed in the upper end of the tank, this end will become warmer when the tank is only partially full. A temperature higher than -195° C means that the tank is nearly empty.

The pressure in the dewar is measured by a Pirani gauge and the output is interpreted and displayed by a auxiliary electronics box. The gauge and display are calibrated for each other - changing one of the components can result in very misleading output. In spite of the calibration, the display of pressures below 10^{-3}mBar are somewhat deviating. The Pirani output has been compared to the outputs from Penning sensors of two different brands, which are more reliable in this pressure range. The relation between Penning and Pirani pressure is shown in figure 12. The repeatability of the measurements are apparently not very good, but when the display shows less than 10^{-3} mBar, it seems safe to consider the displayed pressure an upper limit to the actual pressure. Beware that at pressures near atmospheric pressure, the display may show a too small pressure by a factor of around three. This should especially be considered when filling the dewar with dry air from a pressurized bottle.

The dewar is equipped with a activated charcoal sieve, which will help to keep the vacuum when cold. The operating pressure should be below 10^{-3}mBar. If the pressure goes above this while the camera is cold, the dewar should be pumped for a day at room temperature to evacuate the sieve. If the CCD temperature goes above -50° C, the Oxygen soaking must be repeated.

References

[Andersen, M. I. 96] Andersen, Michael I. & Sørensen, Anton N. : **An interferometric method for measurement of the detector MTF**, ESO Workshop on optical detectors for astronomy, in press.

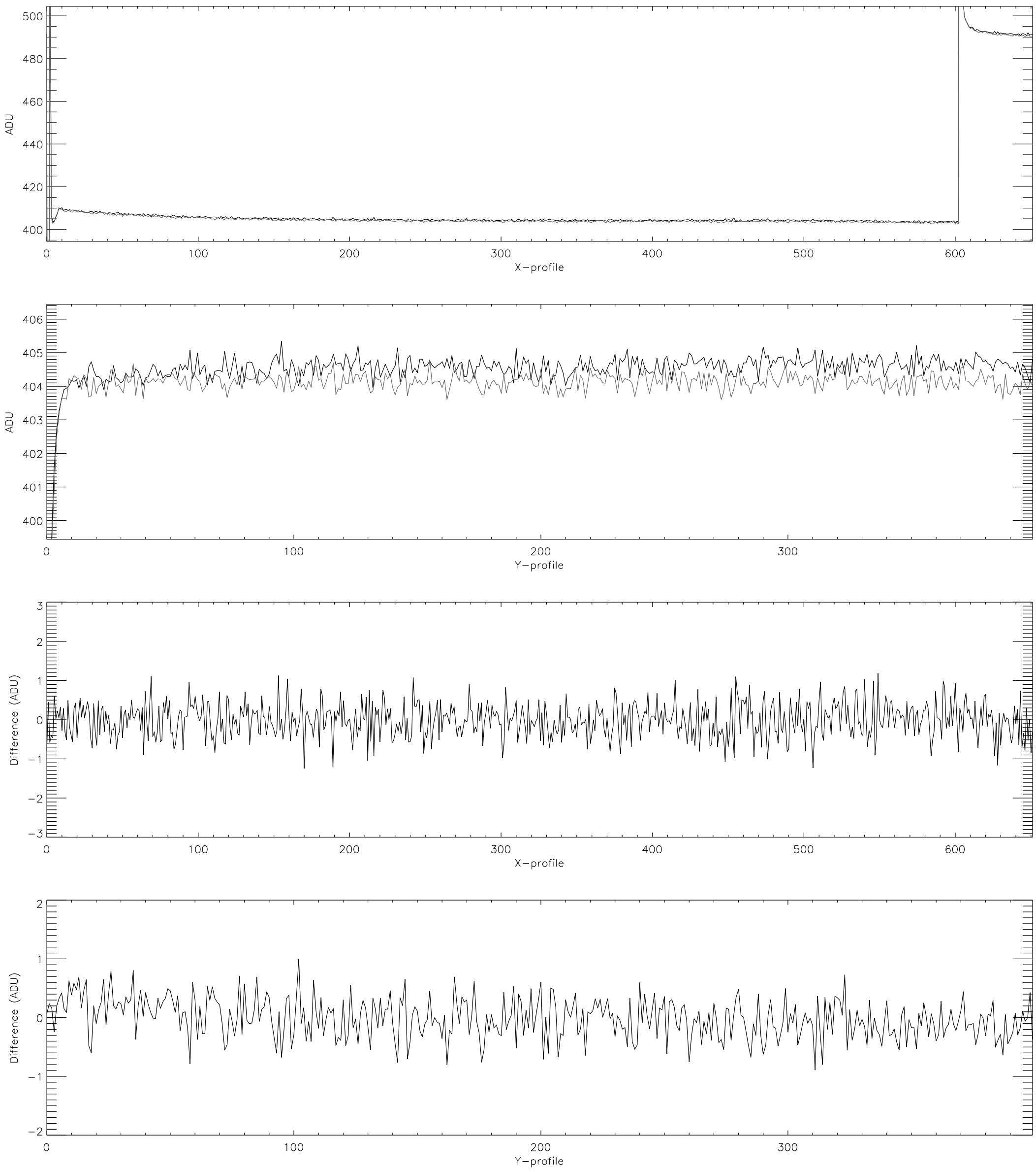

Figure 9: At the upper plot, the X-profiles of two bias frames are displayed. In black is drawn a frame taken after an idle time of an hour, in grey a frame taken after a period with continuous read-out. From column 552 to 602 is the "xover" type overscan, and from column 602 to 652 the "over" type that is strongly offset in level. In the plot below, the Y-profiles are shown, and in the two plots at the bottom, the differences between the profiles are shown. The difference between the bias frames is evidently rather small, and both overscan types track the bias level well. If the read-out window does not extend over the edge of the CCD, the "xover" type will not be available, and the "over" type will be unreliable.

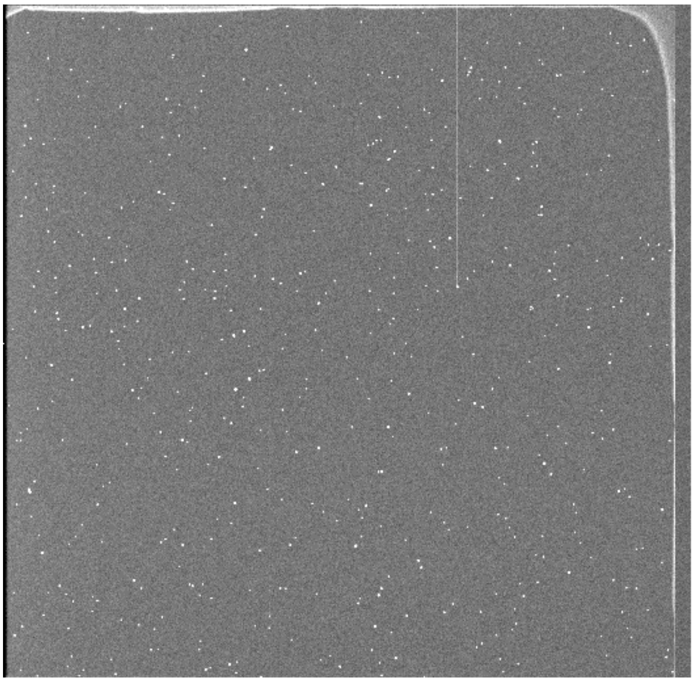

Figure 10: A 20 minute dark exposure. Outside the thick edges and the single hot column, dark current is low and uniform. Cosmic hits appear stellar-like due to the poor MTF.

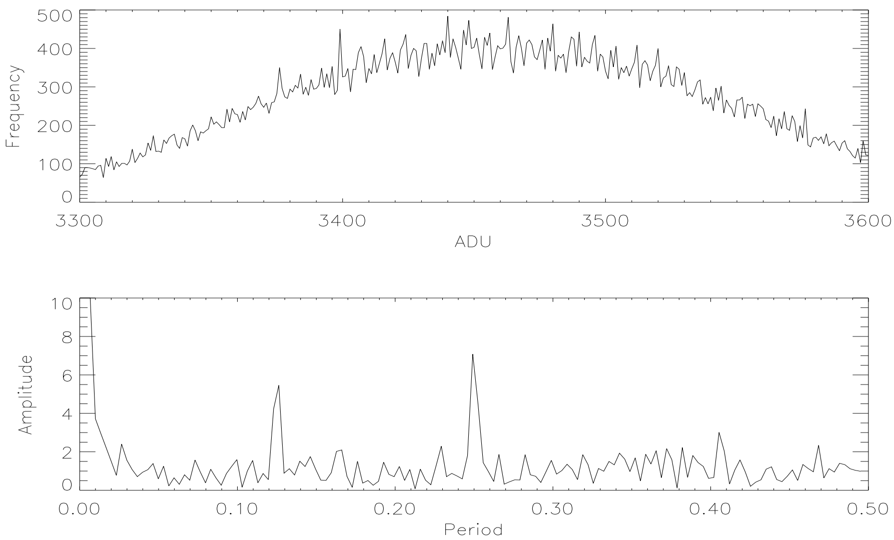

Figure 11: *Upper:* Histogram of a flat-field exposure. *Lower:* Frequency spectrum of the histogram. The ADU levels are seen to be modulated, in particular every fourth and eighth value seems to appear with increased frequency. This is caused by errors in the digitization process.

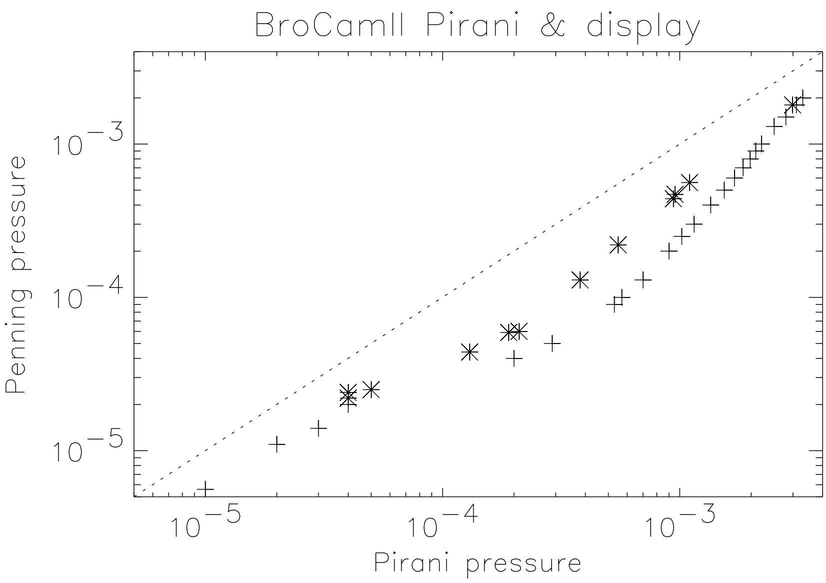

Figure 12: Dewar #2 Pirani sensor pressure versus Penning sensor pressure. Measurements at to different times are shown - the repeatability is apparently not that good.